Development of Cohesive Zone Models for the Prediction of Damage and Failure of Glass/Steel Adhesive Joints

Ioannis Katsivalis[a,b,*], Ole Thybo Thomsen[a], Stefanie Feih[b] and Mithila Achintha[a]

[a] Faculty of Engineering and Physical Sciences, University of Southampton, Southampton SO17 1BJ, UK

[b] Joining Technology Group, Singapore Institute of Manufacturing Technology (SIMTech), 71 Nanyang Drive, Singapore 638075

Keywords: B. Glass, C. Fracture toughness, C. Finite element stress analysis D. cohesive zone model, double cantilever beam, single leg bending

The use of mild steel/tempered glass adhesive joints has increased rapidly over recent years. Cohesive zone modelling (CZM) is used extensively for the numerical analysis and failure prediction of adhesive joints. The bonding to the glass surface is generally weaker than the bonding to metal substrates, and therefore the development of cohesive laws by testing on different substrates generally leads to overoptimistic and non-conservative predictions. However, the interface characterisation using standardised methods for glass/steel joints is complicated due to the relatively low strength of the glass substrate leading to premature failure. This paper presents modifications proposed for the Double Cantilever Beam (DCB) and End Notched Flexure (ENF) tests bonded with dissimilar glass/steel adherends and used to extract traction-separation laws in fracture modes I and II. For this relatively small coupon size, an in-house glass heat strengthening process was developed. The cohesive laws were validated by comparing the numerical predictions for two different adhesives with experimental test data for double lap shear joints subjected to four different load cases.

1. Introduction

The use of glass in the construction industry has increased rapidly in recent years [1, 2]. However, a number of challenges remain when glass is used as a structural material [3]. For instance, the uncertainty and the relatively low strength of glass in combination with its brittleness makes the use of glass challenging. In addition, an effective and durable connection method is currently lacking, while at the same time the numerical analysis of these connections is not always straightforward. Stress concentrations should generally be avoided in glass structures, but they are typically present in the vicinity of load introduction and connection points. Mechanical fasteners are being used extensively, but lack structural efficiency [3]. Adhesive joints are an appealing alternative, but their strength and failure analysis is

*Corresponding author
Email addresses: i.katsivalis@soton.ac.uk (I. Katsivalis), O.Thomsen@soton.ac.uk (O.T. Thomsen), feihs@simtech.a-star.edu.sg (S. Feih), Mithila.Achintha@soton.ac.uk (M. Achintha)

complicated due to complex material characteristics under different loading conditions, and the durability of these joints under environmental conditions remains an active field of research.

Adhesive joints are typically analysed using Finite Element (FE) methods employing continuum mechanics approaches, and the prediction of joint failure is typically based on multiple criteria for the constituent materials including, but not limited to, maximum principal stress, maximum strain and ductile damage. These element-based failure criteria have been used extensively in the past [4-10] but inhibit significant disadvantages: they are mesh size-dependent [11, 12], assume perfect bonding between the substrates and the adhesive, and they generally adopt the bulk properties of the constituent materials as model input.

An alternative to continuum mechanics approaches that has been widely adopted recently for the modelling of bonded connections, is the use of Cohesive Zone Models (CZM). Traction-separation laws are used to characterise the bonded substrate-adhesive interface and this type of analysis is mostly mesh size independent since energetic criteria govern the crack growth [13]. However, the quantitative determination of cohesive laws under different failure modes can be challenging. Traction-separation laws are sensitive to the surface chemistry of the substrates used and also to the bondline thickness.

The determination of the cohesive properties (traction and fracture toughness) in mode I is typically achieved using the Double Cantilever Beam (DCB) [14-16]. ASTM D3433-9 describes the DCB test for similar metal substrates, and the method has been used extensively for interface characterization. For the determination of the cohesive properties for mode II loading, the End Notched Flexure (ENF) test is generally used [17-19].

In the case of hybrid glass/steel adhesive joints, CZM models should be derived for the same dissimilar substrates as utilized for the actual joint configuration to accurately capture relevant surface chemistry effects. However, due to the relatively low strength of the coupon-sized glass substrates, which cannot generally be tempered, the characterisation of the interface properties in fracture/separation modes I and II as per ASTM standards results in glass substrate failures.

CZM approaches adopted for glass/steel connections have therefore been limited to calibrating the traction-separation laws to match the experimental joint strength data, rather than performing data extraction from interface characterisation testing [20]. Other numerical analyses on glass/steel adhesive joints have been limited to continuum mechanics approaches, such as presented in [21-25]. Hence, a robust and validated methodology for the characterisation of hybrid glass/steel adhesive interfaces in bonded joints loaded in modes I and II is currently lacking.

In this paper, we resolved the problem of substrate failure by two means: (1) the stresses in the DCB/ENF substrates were reduced and (2) the glass substrate strength was increased. For the former, the DCB geometry was numerically optimized to minimize the substrate strength. As ENF generally creates significant stresses in both substrates regardless of adherend thickness as per preliminary investigations, the Single Leg Bending (SLB) test [26], a simple modification of the ENF test which introduces mode-mixity [27, 28] and significantly reduces the stresses in the substrates, was used as an alternative. For the latter, a reliable in-house glass heat strengthening process was developed to increase the stress of the relatively small DCB/SLB glass substrates.

The modified and customised DCB and SLB test methodology with hybrid glass and steel substrates was validated for Araldite 2020, which is a brittle epoxy resin, and Araldite 2047-1, which is a ductile methacrylate. Accurate traction-separation law parameters taking into account the hybrid surface chemistry were measured and later validated for glass/steel double lap shear adhesive joints subjected to four typical load cases, namely tension, compression, in-plane and out-of-plane bending. As the dissimilar joints failed at the weaker glass/adhesive interface, we also highlight the ability of our approach to capture this well-known effect experimentally with the CZM parameters, resulting in a reduction in fracture parameters when compared to standard steel/steel joints. Thus, this paper presents for the first time a complete methodology for the characterisation of glass/steel bonded interfaces, from the numerical data extraction from experimental traction-separation results to the experimental validation of these laws in double lap shear joints subjected to quasi-static loading corresponding to four different load cases.

2. Methodology

2.1 Adherend characteristics

Tempered glass is the glass type mostly used in the construction industry, and it was therefore chosen as the main substrate for this study. It has to be noted however, that there is a minimum plate size that glass producers can thermally strengthen. In most cases, the minimum size, readily available in the market, is 100 mm x 250 mm, and therefore this size was chosen for the glass substrates used in the double lap shear joints tested in this work.

However, for the interface characterisation tests (DCB and SLB), smaller glass substrates were needed. Here, annealed glass had to be purchased due to size constraints. However, the strength capacity of annealed glass is significantly lower than that of tempered glass. Preliminary

numerical and experimental studies showed that the stresses generated in the glass substrate during interface testing significantly exceeded the strength of annealed glass. Therefore, a methodology was developed in-house to thermally strengthen the annealed glass.

A furnace was used for the in-house heat strengthening process, and it was attempted to copy the technical procedures that glass manufacturers are using for glass tempering [2, 3]. The annealed glass specimens were heated up to 650°C and then quickly removed from the furnace and sprayed with jets of cold air. Figure 1 shows that the adopted method led to a strength increase of approximately 75% compared to the as-purchased, annealed glass substrates when tested under 3-point bending. The result of the in-house heat strengthening compared to the typical 200% strength increase [3] that can be achieved in automated tempering processes is relatively low, but the strength increase was adequate for the completion of the DCB and SLB tests since glass failure was eliminated.

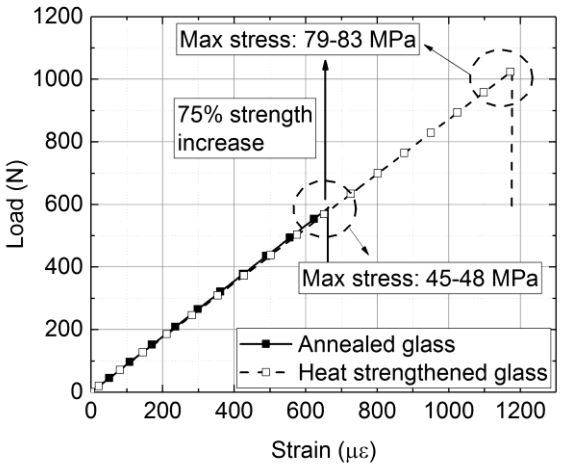

Figure 1: Effect of in-house strengthening on glass failure load under 3-point bending loading

Mild steel was used for the manufacturing of the hybrid joints tested. For the stiffness and strength of the mild steel (Young's modulus and yield stress), standard textbook values were assumed [29]. In the analyses that follow, the stresses generated in the mild steel were

significantly lower than the yield/failure stresses, and therefore plasticity/failure of steel was not considered. Table 1 shows the main material properties that were used in the experimental and numerical work of this project.

Table 1: Properties of the materials used in the numerical and experimental work

Material properties			
Material	E [GPa]	v [-]	Failure/yield Stress [MPa]
Tempered Glass[1]	70	0.23	120
Mild Steel[2]	210	0.3	400

[1] Haldimann, Luible [3], [2] Oberg and McCauley [29]

2.2 Adhesives characteristics

Two adhesives with different characteristics were used in this study: (1) Araldite 2020 (Huntsman; Basel, Switzerland [30]), a 2-Part clear epoxy resin, and (2) Araldite 2047-1 (Huntsman; Basel, Switzerland [31]), a 2-Part methacrylate. These two adhesives were investigated previously by the authors [32], and their mechanical properties are summarised in Table 2.

Table 2: Results of material characterization testing for Araldite 2020 and Araldite 2047-1 [32]

	Araldite 2020 (Brittle)	Araldite 2047-1 (Ductile)
Resin system	Epoxy	Methacrylate
Young's modulus (E)	2.57 ± 0.08 GPa	0.89 ± 0.084 GPa
Poisson's ratio (v)	0.38 ± 0.004 (-)	0.42 ± 0.001 (-)
Tensile yield strength (σ_{yT})	31.33 ± 2.73MPa	5.56 ± 0.11 MPa
Tensile failure stress (σ_{fT})	45.39 ± 2.61MPa	13.1 ± 1.13 MPa
Tensile failure strain (ε_{fT})	3.1 ± 0.6(%)	17 ± 4.1 (%)

From Table 2 it is seen that the two adhesives have significantly different behaviour, and based on their characteristics Araldite 2020 will be referred to as a brittle adhesive, while Araldite 2047-1 will be referred to as a ductile adhesive in this work.

2.3 Numerical methodology

CZM is used for the simulation of the elastic region, damage initiation, damage evolution and final failure of an interface. Traction-separation laws relate stresses to relative displacements of the nodes of the cohesive elements. Traction-separation laws can have different shapes, but generally the elastic deformation of a material is followed by a peak value of stresses after which the damage initiates leading to complete failure after a given relative displacement [19, 33]. The area under each traction-separation law graph represents the fracture energy of the interface.

The main types of cohesive laws that are typically adopted are triangular, exponential and trapezoidal [19, 33]. Generally, the triangular CZM shape is mostly used for brittle adhesives with small plastic deformations after yielding [13]. The trapezoidal shape allows for plastic deformations and therefore is more suitable for ductile materials [34]. It is worth noting that a direct method can also be used for the extraction of the exact shape of the cohesive laws [16, 35-37], but in this work a simple triangular law was used since it provided good agreement with the experimental data in terms of maximum failure loads and progressive failure response.

Different criteria can be used for the modelling of damage initiation (maximum/quadratic nominal/principal stress/strain) and damage evolution (displacement or energy controlled). In this study, a quadratic nominal stress criterion was used for the damage initiation, following similar studies [13, 27, 34, 38, 39] and is shown in equation (1):

$$\left(\frac{t_n}{t_n^0}\right)^2 + \left(\frac{t_s}{t_s^0}\right)^2 = 1 \quad (1)$$

In equation (1), t_n and t_s are the tensile normal and shear stresses, respectively, while t_n^0 are t_s^0 are the initiation stresses in tension and shear, respectively. It is further assumed that damage is not caused by normal compressive stresses [38]. When equation (1) is fulfilled, the softening process of the material's stiffness begins. In this study, this process is controlled by adopting a linear mode-mixity fracture energetic criterion, following similar studies [13, 38-41] as shown in equation (2):

$$\frac{G_n}{G_n^c} + \frac{G_s}{G_s^c} = 1 \quad (2)$$

In (2) G_n and G_s are the fracture energies in tension and shear while G_n^0 and G_s^0 are the critical fracture energies in modes I and II.

For the numerical simulations, both the implicit and explicit solvers of the commercial finite element (FE) code ABAQUS 6.14 were used. The results presented in the subsequent sections were taken from the explicit solver. However, later analysis revealed that the implicit solver produced similar results.

The substrates were modelled using 3D stress (continuum), 8-node linear solid elements with reduced integration and hourglass control (C3D8R in ABAQUS). In addition, the cohesive layers were modelled with 8-node 3D cohesive elements (COH3D8 in ABQUS). The traction-separation laws were established by developing models for the modified DCB and SLB tests.

In these tests, the adhesive layer was modelled as a single row of cohesive elements representing the bondline thickness.

The cohesive properties were determined using the inverse method [33] performing numerical iterations until good agreement between the experimental and numerical load displacement curves was achieved. During this calibration process the stiffness of the cohesive elements remained constant (values for Young's modulus taken from Table 2) while the traction and fracture energy were varied. The combined numerical and experimental approach for the determination of the cohesive properties (traction and fracture energy) in modes I and II is summarised in Figure 2.

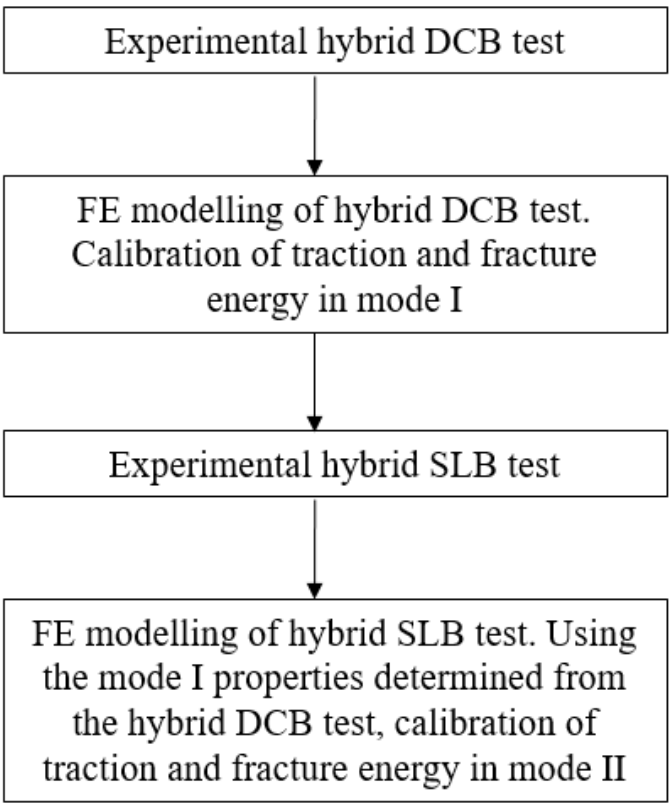

Figure 2: Flowchart describing the experimental and numerical procedure for the determination of the cohesive properties in modes I and II.

3. Interface characterisation tests

3.1 Modified DCB test

Dissimilar substrates were used for the interface characterisation tests, and therefore it was important to match the bending stiffness of the two substrates to ensure that loading was symmetrical and the adhesive layer was deforming in pure mode I. In order to achieve this, the thickness of the two substrates was adjusted such that the thickness of the glass substrate was 12 mm and the thickness of the steel substrate was 8 mm following equation (3):

$$t_1 = \left(\sqrt[3]{E_2/E_1}\right) t_2 \tag{3}$$

In equation (3), t_1 and t_2 are the thicknesses of the glass and the steel substrates, while E_1 and E_2 are the respective values for Young's modulus.

The geometry of the modified DCB specimens and the experimental setup is shown in Figure 3, and the dimensions are displayed in Table 3. A steel fixture was used for the alignment of the substrates, and 0.2 mm steel wires were used for controlling the bondline thickness. The steel substrates were sandblasted before bonding to improve adhesion, and both glass and steel substrates were degreased using acetone. The glass substrates used for these tests were the ones that were strengthened in-house as described in section 2.1. Finally, before joint manufacturing both substrates underwent atmospheric plasma treatment with a mixture of argon and oxygen gas to improve adhesion by surface activation.

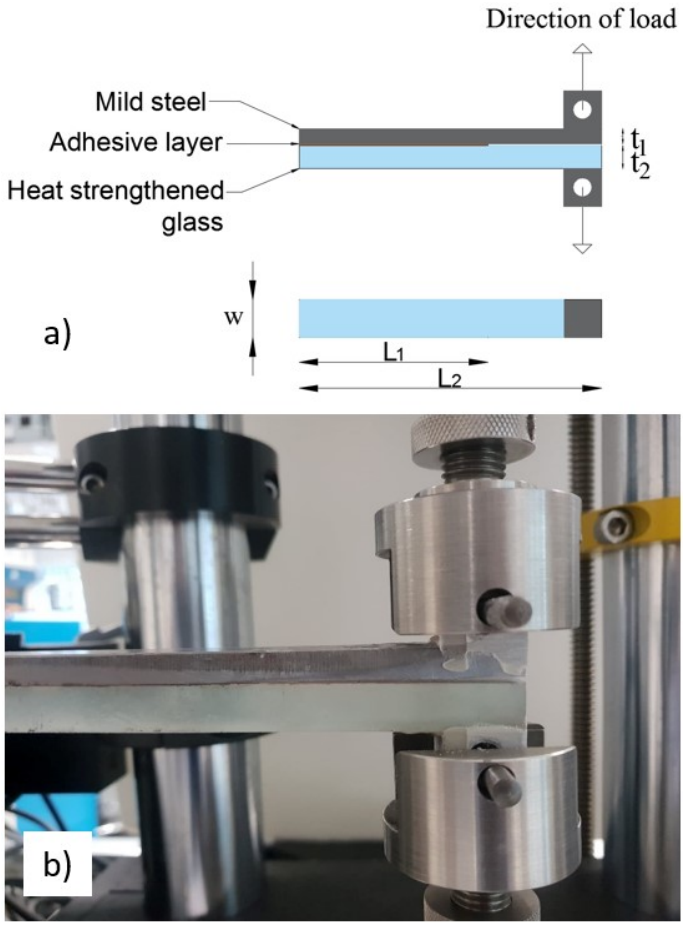

Figure 3: Modified DCB a) design and b) test setup

Table 3: Summary of the geometry of the DCB test

L_1	160 mm
L_2	100 mm
t_1	8 mm
t_2	12 mm
w	20 mm
Bondline thickness	0.2 mm

Finite element analysis of the test set-up was conducted. The set-up presented in Figure 3 produced a symmetrical loading condition and loading in pure mode I. The stress distribution in the substrates during crack initiation is shown in Figure 4. The stresses developed in the glass exceed the nominal strength of annealed glass (~ 40 MPa), but are within the limits of the

in-house heat strengthened glass. Figure 5 shows the typical failure pattern of these specimens with the initially used annealed glass substrate.

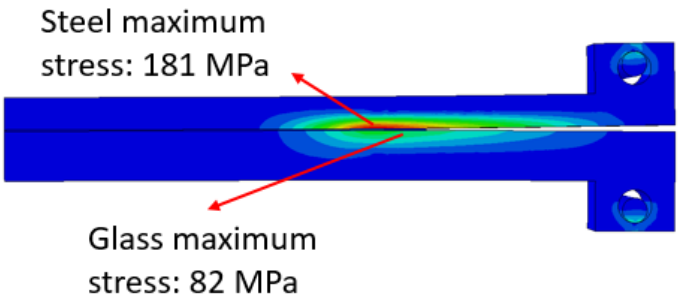

Figure 4: Maximum principal stress distribution at damage initiation for the modified DCB specimen.

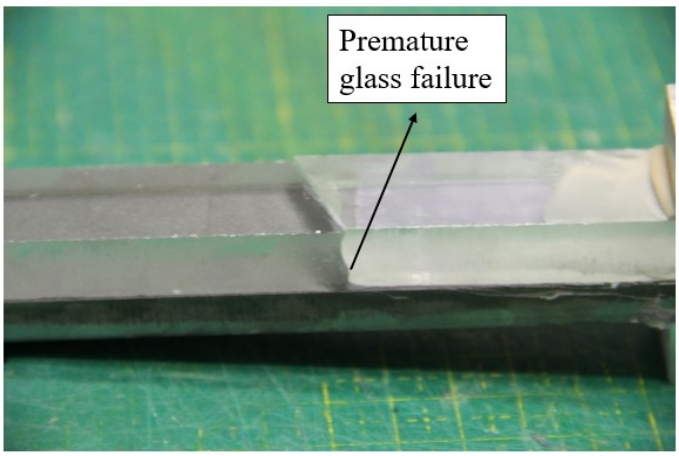

Figure 5: Premature glass failure in the crack tip area

Figure 6 shows typical glass/steel interfaces after failure using the in-house heat strengthened glass substrates. Figure 7 shows characteristic load-displacement curves obtained experimentally for the joints with brittle and ductile adhesives, and also the corresponding FE simulation numerical curve fitting. It was observed that both adhesives failed at the interface, but whilst fully adhesive failure was seen for the brittle adhesive, the ductile adhesive experienced a combination of adhesive and cohesive failure. Analysis of the failed interfaces revealed that the contribution of the cohesive mode of failure was in the range 20-50%, while the contribution of the adhesive mode of failure was in the range 50%-80%.

The different failure mechanisms highlight the importance of the CZM simulation and the calibration of the traction-separation laws on glass/steel interfaces. Table 4 presents a summary of the DCB tests performed, and Table 5 presents the properties that were calibrated numerically for mode I for the two adhesives. The calibration was based on characteristic specimens representing average results for each case. It is highlighted that the calibrated interface properties (Table 5) are different compared to the adhesive properties extracted from tensile tests (Table 2). The differences become more important when the failure mechanism is mostly adhesive.

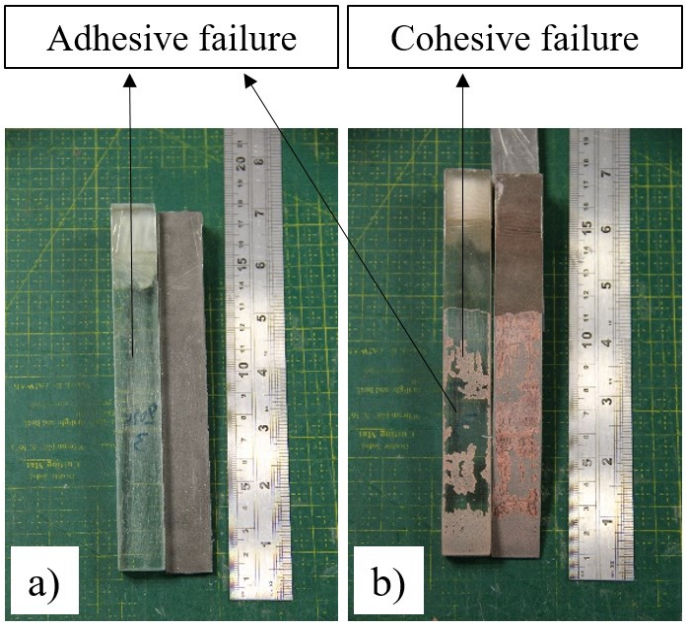

Figure 6: Glass/steel DCB typical interfaces after failure for the brittle (left) and ductile (right) adhesive

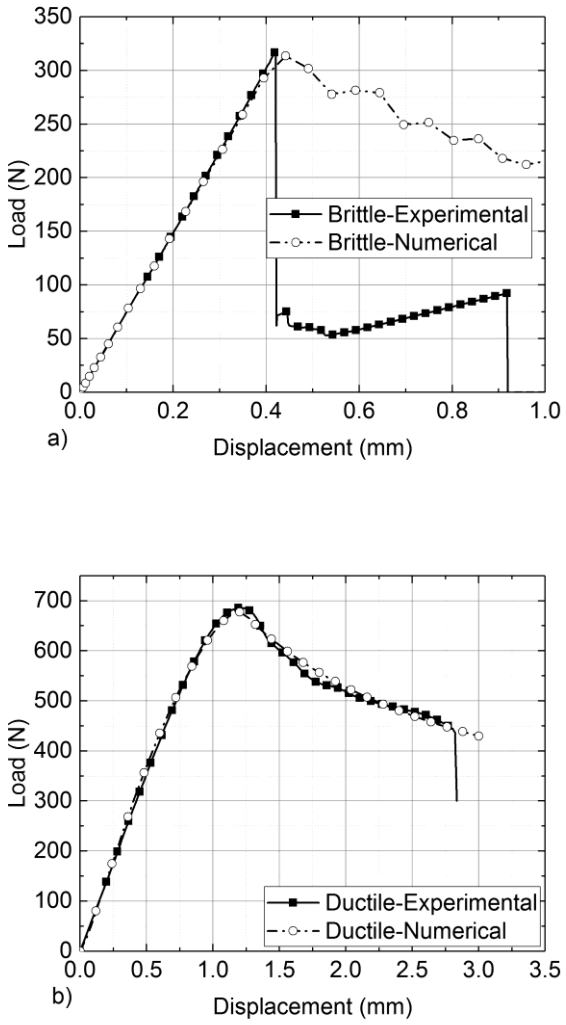

Figure 7: Load-displacement curves for the DCB tests and corresponding FE curve fitting for the a) brittle and b) ductile adhesives

Table 4: Summary table of DCB tests

Specimen	Average Max Load (N)
Araldite 2020 (Brittle)	286 ± 55
Araldite 2047-1 (Ductile)	649 ± 29

Table 5: Cohesive properties in loading mode I for the two adhesives for dissimilar glass/steel joints (fitted with triangular cohesive law)

Property	Araldite 2020 (Brittle)	Araldite 2047-1 (Ductile)
E (GPa)	2.57	0.89
t_n (MPa)	25	10
δ_n (mm)	0.004	0.104
G_n^c(J/m^2)	50	520

Figure 7 shows that for the brittle adhesive a sudden load drop occurred after damage initiation (maximum load). This indicates that the crack did not propagate progressively, but that a significant length of the interface debonded instantly. Therefore, the calibration of the cohesive properties was only based on the maximum load. In contrast, for the ductile adhesive the damage propagated progressively, and the numerical calibration was based on both the maximum load and the load drop region. It is noted that both traction and fracture energy influence the maximum load while the slope of the load drop region is affected only by the fracture energy.

It is important to highlight that steel or aluminium substrates could be used to perform the same tests and avoid the premature glass failures as per ASTM standards. However, assuming that the interface response between glass/steel and steel/steel behaves in a similar manner was a simplification that could not be physically justified, and was assumed to lead to overestimations of the cohesive law parameters and thus the strength of the joints. To demonstrate this, the response of the glass/steel DCB specimen was compared with a steel/steel DCB specimen for both the brittle and the ductile adhesive. The differences are shown in Figure 8.

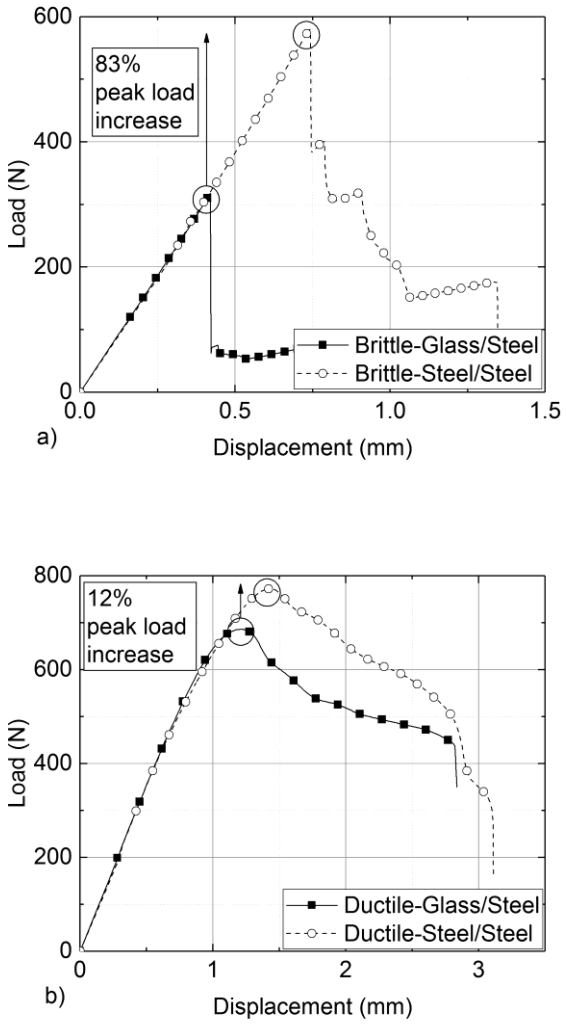

Figure 8: Load-displacement response of glass/steel and steel/steel DCB specimens for the a) brittle and b) ductile adhesives.

It is observed from Figure 8 that the glass/steel DCB specimens failed at lower loads compared to the steel/steel joints. The steel/steel DCB specimen with the brittle adhesive failed at 83% higher loads compared to the glass/steel specimen. Similarly, for the ductile adhesive, the strength increase was 12% for steel/steel joints relative to steel/glass joints. In addition, the steel/steel specimens failed mostly cohesively, while for the steel/glass specimens mixed adhesive/cohesive failure was observed. Accordingly, considering the correct substrate configuration for CZM evaluation is important in order to capture the effects of surface chemistry and substrate/adhesive bonding.

3.2 Modified SLB test

SLB is a simple modification of the ENF test that introduces mode-mixity in the adhesive layer, and also drastically reduces the stresses in the substrates, especially in the bottom substrate. The thickness of the two substrates determines the influence of modes I and II during the test. Finite element analysis was again conducted to determine the optimum thickness of the two substrates, aiming to keep the tensile stresses generated in the glass substrate below 40 MPa to avoid the need for heat strengthening. Figure 9 shows the typical stress results of the chosen geometry highlighting the maximum principal stresses in the glass and steel substrates.

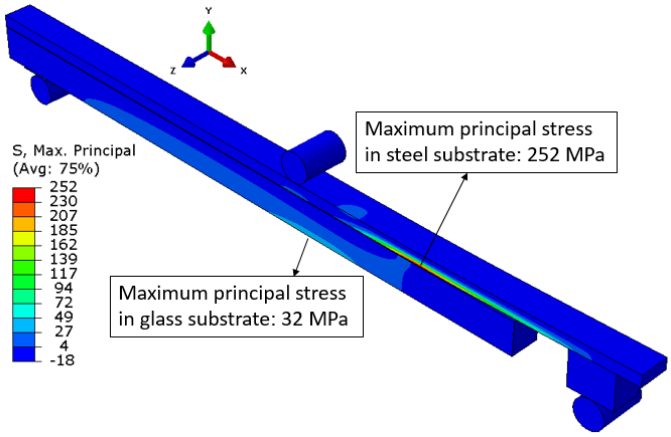

Figure 9: Preliminary FE analysis for the SLB test aiming to minimise the stress distribution in the glass substrate. Symmetry in the z axis is used.

The final geometry of the SLB specimen and the experimental setup can be found in Figure 10, and the dimensions are given in Table 6. Similarly to the DCB test, a steel fixture was used for the alignment of the substrates, and 0.2 mm wires were used for controlling the bondline thickness. Load-displacement curves were recorded during the tests and subsequently compared with the FE simulation results. The CZM properties for mode I also needed to be included in the simulation due to the mode-mixity of the configuration. The comparison

between the experimental observations and the numerical simulations led to the calibration of the traction-separation law for mode II loading.

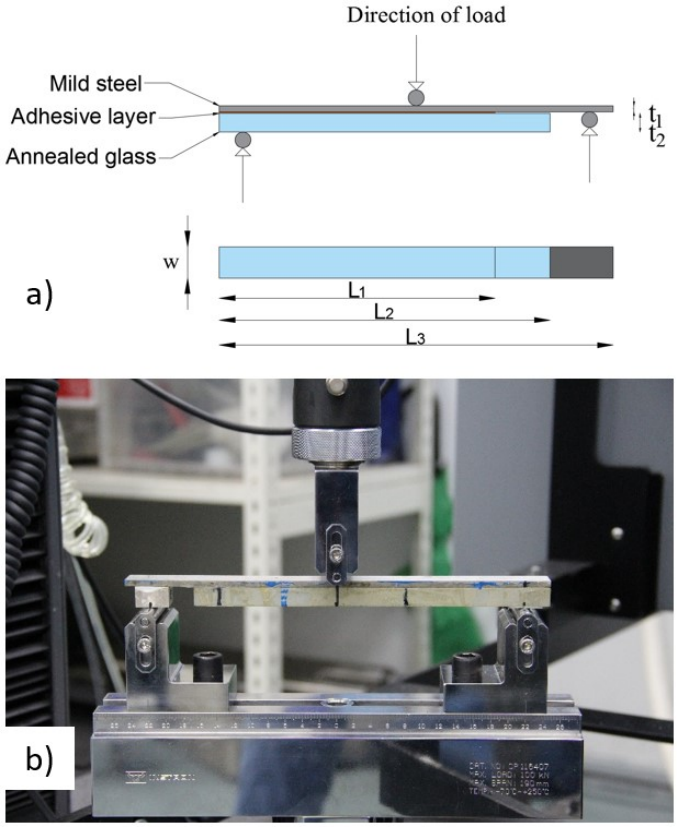

Figure 10: SLB a) design and b) test setup

Table 6: Summary of the geometry of the SLB test

L_1	180 mm
L_2	210 mm
L_3	250 mm
t_1	4 mm
t_2	12 mm
w	20 mm
Bondline thickness	0.2 mm

Figure 11 shows typical specimens of each adhesive type after failure. It is observed that in all cases the damage is adhesive/cohesive. Furthermore, it is hard to distinguish between the two as the specimens were still bonded together after the tests were conducted. Figure 12 shows characteristic load-displacement curves obtained for the two types of adhesive. The sudden load drops indicate adhesive damage, while the gradual load drops indicate progressive damage in the adhesive layer, thus providing evidence of a process that involves a combination of adhesive and cohesive damage. Table 7 summarises the SLB tests performed, and Table 8 presents the properties that were calibrated numerically for mode II loading for both adhesive types.

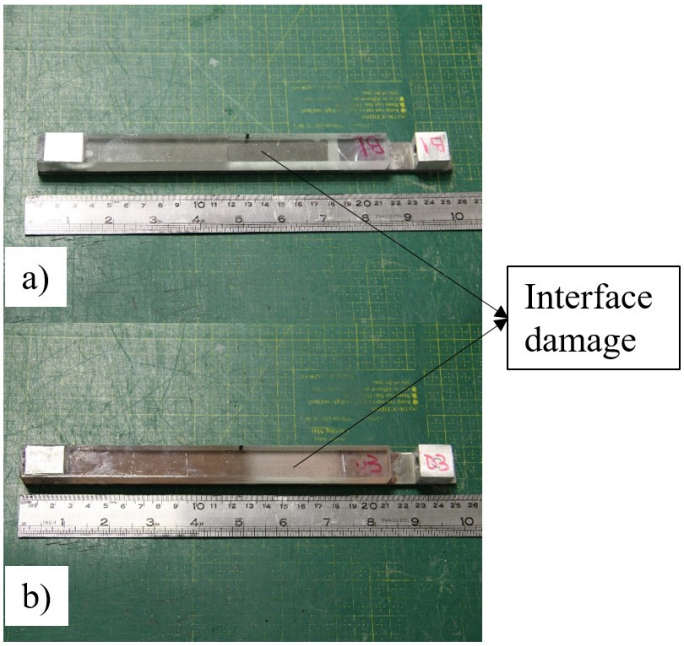

Figure 11: Glass/steel SLB typical interfaces after failure for the (a) brittle and (b) ductile adhesive

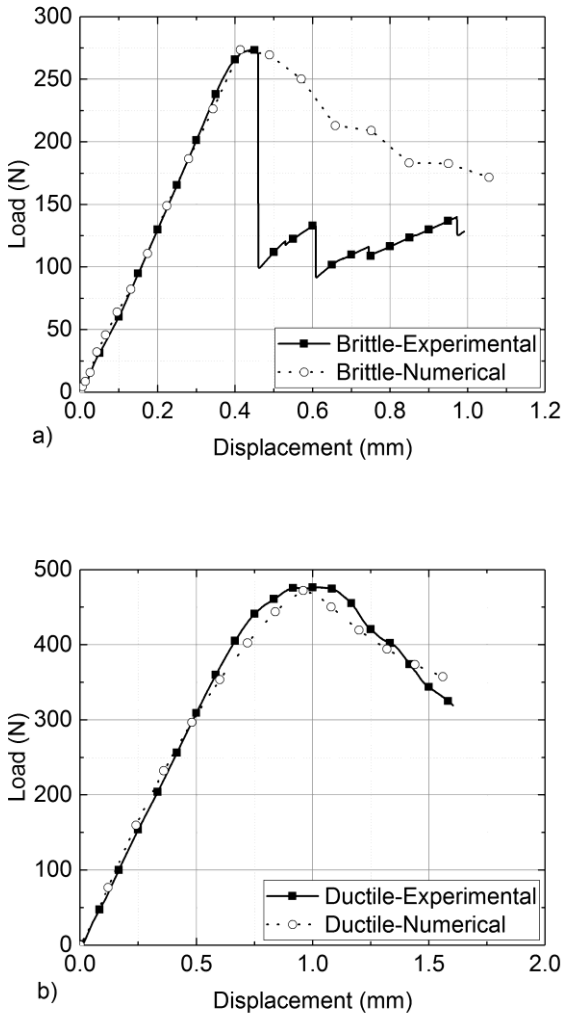

Figure 12: Load-displacement curves for the SLB tests and corresponding FE curve fitting for the (a) brittle and (b) ductile adhesives

Table 7: Summary table of SLB tests

Specimen	Average Maximum Load (N)
Araldite 2020 (Brittle)	254 ± 21
Araldite 2047-1 (Ductile)	419 ± 45

Table 8: Cohesive properties in mode II for the brittle and ductile adhesives (fitted with triangular cohesive laws)

Property	Araldite 2020 (Brittle)	Araldite 2047-1 (Ductile)
G (GPa)	0.93	0.31
t_s (MPa)	15	2
δ_s (mm)	0.013	1.04
G_s^c (J/m^2)	100	1040

During the SLB tests a sudden load drop was recorded once the brittle adhesive reached its maximum load, similar to the DCB tests. Therefore, the properties for mode II were again calibrated against the maximum load reached during the SLB test. For the ductile adhesive however, damage propagated gradually and a smooth load drop was observed leading to the calibration of the cohesive properties in mode II. Once again, the sudden load drops indicate rapid interface (adhesive) failure, while a smooth load drop indicates mostly cohesive damage.

4. Validation of cohesive laws in shear joints

The calibrated cohesive laws were evaluated with respect to their predictive capabilities for double lap shear joints connecting the tempered glass substrates to mild steel. Details regarding the experimental campaign can be found in [42]. Figure 13 presents the design of the joints and the load configurations tested.

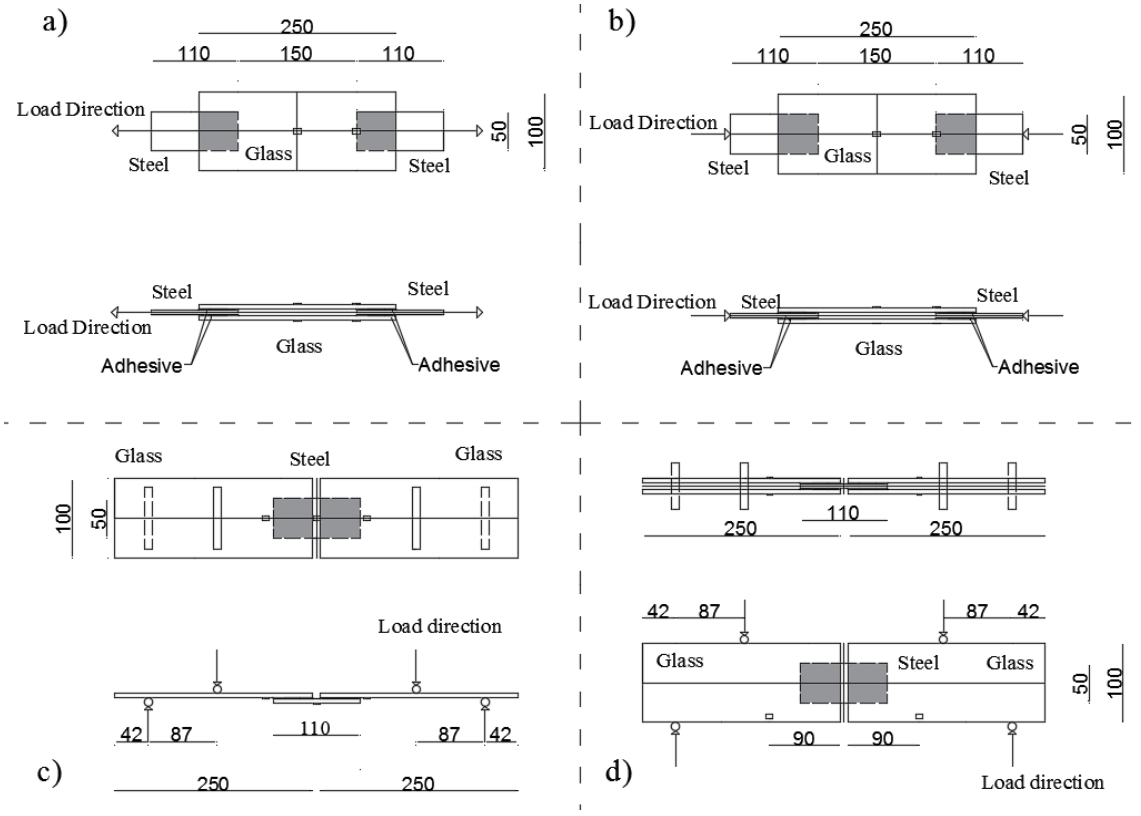

Figure 13: Design details of the uniaxial a) tension and b) compression, c) out-of-plane and d) in-plane bending tests and locations of the strain gauges

A continuum mechanics approach was previously successfully validated by the authors [42], but required extensive mesh size calibration. Here, the numerical validation was based on the failure load predictions using the CZM approach. It is worth noting that cohesive zone models are insensitive to mesh size [11, 12]. Nevertheless, a mesh sensitivity study was carried out to validate this assumption. Figure 14 presents the effect of the mesh size on the predicted failure load for the double lap shear joints subjected to tension.

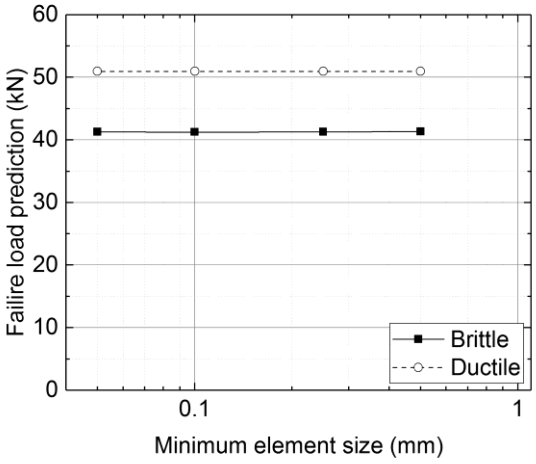

Figure 14: Effect of cohesive element size on the failure load prediction for the brittle and ductile double lap shear joints under tensile loading

From Figure 14 it is observed that the cohesive element size had no notable effect on the predicted failure loads for both the brittle and the ductile adhesives. Therefore, relatively coarser FE meshes could be used in CZM analysis, reducing the computational time significantly but not affecting the accuracy of the predictions. This is a significant advantage compared to the continuum mechanics approach.

The numerical validation presented was based on comparison between the predicted failure loads obtained using the CZM models and the experimental measurements. Tables 9 and 10 show the experimental measurements relating to the failure of the joints as well as the numerical predictions for uniaxial tension and compression loading. Furthermore, Figure 15 shows the joint response measured by strain gauges and predicted numerically in the midpoint of the joint for both the uniaxial tension and compression load cases.

Table 9: Summary of experimental and numerical results for the double lap shear joints with brittle and ductile adhesives subjected to tensile loading

	Tension			
	Experimental		Numerical	
	Failure load (kN)	Failure mechanism	Failure load (kN)	Failure mechanism
Araldite 2020 (Brittle)	38.0 ± 1.8	Significant damage in the adhesive layer/interface leading to glass failure	40.4	Interface failure (failure of cohesive elements)
Araldite 2047-1 (Ductile)	47.0 ± 4.6	Cohesive failure	50.8	Interface failure (failure of cohesive elements)

Table 10: Summary of experimental and numerical results for the double lap shear joints with brittle and ductile adhesives subjected to compressive loading

	Compression			
	Experimental		Numerical	
	Failure load (kN)	Failure mechanism	Failure load (kN)	Failure mechanism
Araldite 2020 (Brittle)	42.4 ± 5.1	Significant damage in the adhesive layer/interface leading to glass failure	40.8	Interface failure (failure of cohesive elements)
Araldite 2047-1 (Ductile)	45.5 ± 0.7	Cohesive failure	50.8	Interface failure (failure of cohesive elements)

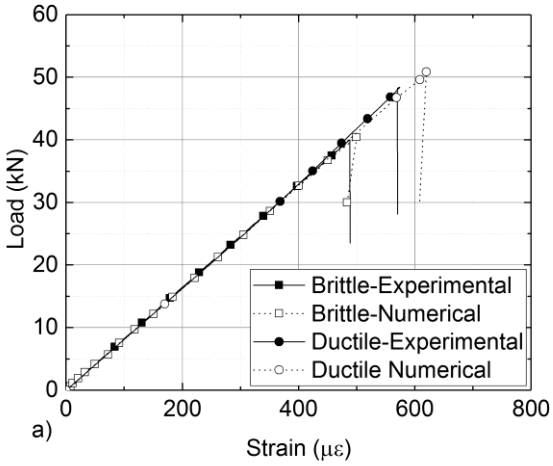

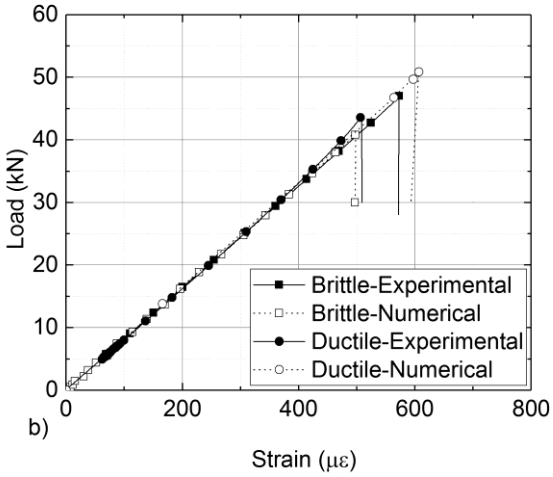

Figure 15: Load response of double lap shear joints– experimental measurements and numerical predictions for a) tensile and b) compressive loading.

It can be seen that the measured and implemented cohesive laws provided accurate predictions for both adhesive types when subjected to both uniaxial tensile and compressive loading. Moreover, the CZM model predictions accurately captured that failure occurs in the interface and only overestimated the failure load by 7% and 8% for the brittle and ductile adhesives, respectively. For compressive loading, failure was predicted to occur in the interface, and the failure load was underestimated by 4% for the brittle adhesive and overestimated by 11% for the ductile adhesive. Finally, the strain response of the joints predicted by the CZM models matched the experimental data very closely.

Tables 11 and 12 show the experimental data of the failure of the joints as well as the numerical predictions for the lap shear joint configurations subjected to in-plane and out-of-plane bending loading. Furthermore, Figure 16 shows the joint response measured by strain gauges and the corresponding numerical predictions. As was shown in Figure 13, the strain gauge used for the out-of-plane bending test was located in the centre of the joint in the steel substrate, while for the in-plane bending test the strain gauge was located in the tensile side of the glass substrate where the maximum stresses were expected to occur.

Table 11: Summary of experimental and numerical failure results for lap shear joints with brittle and ductile adhesives subjected to out-of-plane bending loading

	Out-of-plane bending			
	Experimental		Numerical	
	Failure load (kN)	Failure mechanism	Failure load (kN)	Failure mechanism
Araldite 2020 (Brittle)	0.83 ± 0.21	Adhesive/cohesive failure	0.98	Interface failure (failure of cohesive elements)
Araldite 2047-1 (Ductile)	1.45 ± 0.04	Glass failure	1.52	Glass failure

Table 12: Summary of experimental and numerical failure results for lap shear joints with brittle and ductile adhesives subjected to in-plane bending loading

	In-plane bending			
	Experimental		Numerical	
	Failure load (kN)	Failure mechanism	Failure load (kN)	Failure mechanism
Araldite 2020 (Brittle)	14.3 ± 0.7	1) Adhesive/cohesive failure 2) Glass failure preceded by significant damage in the adhesive layer	12.1	Interface failure (failure of cohesive elements)
Araldite 2047-1 (Ductile)	20.0 ± 0.4	1) Adhesive/cohesive failure 2) Glass failure preceded by significant damage in the adhesive layer	18.8	Interface failure (failure of cohesive elements)

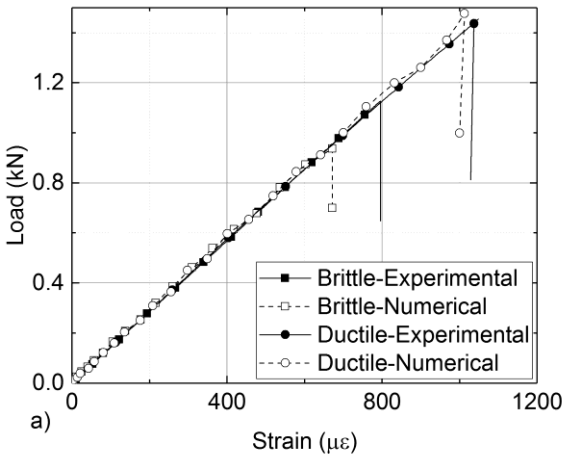

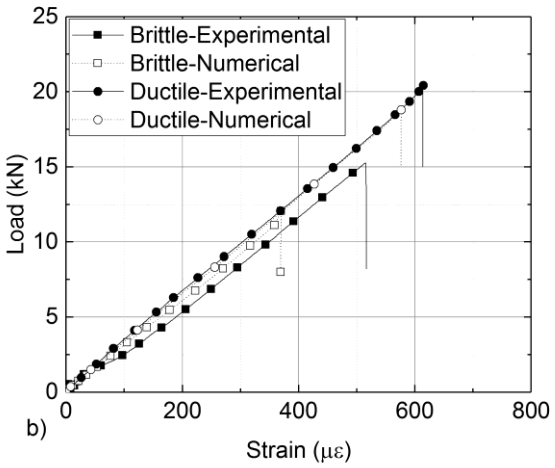

Figure 16: Load response of double lap shear joints– experimental measurements and numerical predictions for a) out-of-plane bending and b) in-plane bending loading.

For the case of out-of-plane bending load case, the failure occurred in the interface for the brittle adhesive and in the glass substrate for the ductile adhesive. For both cases, the CZM model predicted the failure mechanism accurately, while the failure load predicted by the CZM model was 17% lower for the brittle adhesive and 6% lower for the ductile adhesive relative to the experimental measurements. However, it should be noted that for the ductile adhesive the damage observed depended entirely on the strength of the glass substrate, since the cohesive damage initiation criterion was not activated when the glass failed.

For the in-plane bending test, the predicted failure location was accurately predicted by the CZM simulation to be in the interface for both joints. Relative to the experimental observations, the predicted failure load was 17% higher for the brittle adhesive and less than 5% higher for the ductile adhesive. Finally, the strain response of the joints predicted by the CZM models matched the experimental measurements accurately.

5. Conclusions

A novel combined experimental and numerical methodology for the development of cohesive zone model parameters for hybrid glass/steel interfaces was presented. For the interface characterisation, two different tests were required with hybrid glass/steel substrates to capture mode I and mode II fracture properties. The first test was a modified Double Cantilever Beam (DCB) test, in which the adhesive layer was loaded in pure mode I, while the second test adopted was a modified Single Leg Bending (SLB) test introducing mode-mixity. Using these two tests, the traction-separation laws in modes I and II could be obtained without premature substrate failure. This achievement required the development of an in-house heat strengthening process suitable for small glass coupons, which increased the glass strength by 75%.

An experimental campaign was carried out to develop triangular traction-separation laws for two different adhesive systems, a brittle epoxy resin and a ductile methacrylate. The cohesive laws were validated with four different load-cases that are frequently encountered in glass structures, i.e. tension, compression, in-plane and out-of-plane bending. The comparison of the experimental and numerical results showed that the developed numerical CZM methodology accurately captured the stiffness response, maximum failure load and failure mechanisms for the investigated glass/steel adhesive joints.

The CZM methodology offered significant advantages over classic continuum mechanics approaches, since the numerical simulations were not mesh size dependent and could accurately simulate damage initiation and propagation criteria for both the implicit and the explicit ABAQUS solvers. Accordingly, the CZM approach and methodology provided significant improvements with respect to computational efficiency and processing time reduced.

Finally, it is noted that the validated cohesive laws for the given hybrid substrates depended on the bondline thickness, the substrate constituent materials and the surface chemistry. For the latter, our research showed that steel/steel adhesive joints were significantly stronger than glass/steel adhesive joints connections. Accordingly, it was essential that the traction-separation laws were derived from dissimilar hybrid substrates and accurate bondline geometries to capture all interface characteristics. It is envisaged that this method can also easily be extended to determine interface properties following moisture and temperature degradation; this is the subject of current research.

Acknowledgements The principal author gratefully acknowledges the funding from the Agency for Science, Technology and Research (A*STAR), Singapore, and the University of Southampton, UK, that has enabled the conduction of the research reported.

References

[1] Achintha M., 5 - Sustainability of glass in construction, in: Khatib J.M. (Ed.), Sustainability of Construction Materials (Second Edition), Woodhead Publishing, 2016, pp. 79-104.

[2] IStructE, Structural use of glass in buildings, Second edition. ed., Institution of Structural Engineers, SETO, London, 2014.

[3] Haldimann M., Luible A., Overend M., Structural use of glass, International Association for Bridge and Structural Engineering, Zürich, Switzerland, 2008.

[4] Adams R.D., Comyn J., Wake W.C., Structural adhesive joints in engineering, 2nd ed., Chapman & Hall, London, 1997.

[5] Zhao X., Adams R.D., da Silva L.F.M., Single Lap Joints with Rounded Adherend Corners: Stress and Strain Analysis, Journal of Adhesion Science and Technology, 25 (2011) 819-36.

[6] Zhao X., Adams R.D., da Silva L.F.M., Single Lap Joints with Rounded Adherend Corners: Experimental Results and Strength Prediction, Journal of Adhesion Science and Technology, 25 (2011) 837-56.

[7] da Silva L.F.M., Carbas R.J.C., Critchlow G.W., Figueiredo M.A.V., Brown K., Effect of material, geometry, surface treatment and environment on the shear strength of single lap joints, Int J Adhes Adhes, 29 (2009) 621-32.

[8] da Silva L.F.M., das Neves P.J.C., Adams R.D., Wang A., Spelt J.K., Analytical models of adhesively bonded joints—Part II: Comparative study, Int J Adhes Adhes, 29 (2009) 331-41.

[9] Crocombe A.D., Global yielding as a failure criterion for bonded joints, Int J Adhes Adhes, 9 (1989) 145-53.

[10] Nguyen A.T.T., Pichitdej N., Brandt M., Feih S., Orifici A.C., Failure modelling and characterisation for pin-reinforced metal-composite joints, Compos. Struct., 188 (2018) 185-96.

[11] Dragoni E., Mauri P., Intrinsic static strength of friction interfaces augmented with anaerobic adhesives, Int J Adhes Adhes, 20 (2000) 315-21.

[12] Feih S., Shercliff H.R., Adhesive and composite failure prediction of single-L joint structures under tensile loading, Int J Adhes Adhes, 25 (2005) 47-59.

[13] Campilho R.D.S.G., Banea M.D., Pinto A.M.G., da Silva L.F.M., de Jesus A.M.P., Strength prediction of single- and double-lap joints by standard and extended finite element modelling, Int J Adhes Adhes, 31 (2011) 363-72.

[14] Fernandes R.L., Campilho R.D.S.G., Testing different cohesive law shapes to predict damage growth in bonded joints loaded in pure tension, The Journal of Adhesion, 93 (2017) 57-76.

[15] de Moura M.F.S.F., Gonçalves J.P.M., Magalhães A.G., A straightforward method to obtain the cohesive laws of bonded joints under mode I loading, Int J Adhes Adhes, 39 (2012) 54-9.

[16] Carlberger T., Stigh U., Influence of Layer Thickness on Cohesive Properties of an Epoxy-Based Adhesive—An Experimental Study, The Journal of Adhesion, 86 (2010) 816-35.

[17] de Moura M.F.S.F., Numerical simulation of the ENF test for the mode-II fracture characterization of bonded joints, Journal of Adhesion Science and Technology, 20 (2006) 37-52.

[18] Borg R., Nilsson L., Simonsson K., Simulating DCB, ENF and MMB experiments using shell elements and a cohesive zone model, Composites Science and Technology, 64 (2004) 269-78.

[19] da Silva L.F.M., Öchsner A., Adams R.D., Handbook of Adhesion Technology: Second Edition, 2018.

[20] Bedon C., Machalická K., Eliášová M., Vokáč M., Numerical Modelling of Adhesive Connections Including Cohesive Damage, Challenging Glass Conference Proceedings, (2018) 309-20%V 6.

[21] Santarsiero M., Louter C., Nussbaumer A., A novel triaxial failure model for adhesive connections in structural glass applications, Engineering Structures, 166 (2018) 195-211.

[22] Santarsiero M., Bedon C., Louter C., Experimental and numerical analysis of thick embedded laminated glass connections, Compos. Struct., 188 (2018) 242-56.

[23] Bedon C., Santarsiero M., Laminated glass beams with thick embedded connections – Numerical analysis of full-scale specimens during cracking regime, Compos. Struct., 195 (2018) 308-24.

[24] Dispersyn J., Belis J., Numerical research on stiff adhesive point-fixings between glass and metal under uniaxial load, Glass Structures & Engineering, (2016).

[25] Santarsiero M., Louter C., Nussbaumer A., Laminated connections under tensile load at different temperatures and strain rates, Int J Adhes Adhes, 79 (2017) 23-49.

[26] Yoon S.H., Hong C.S., Modified end notched flexure specimen for mixed-mode interlaminar fracture in laminated composites, International Journal of Fracture, 43 (1990) R3-R9.

[27] Jung Lee M., Min Cho T., Seock Kim W., Chai Lee B., Ju Lee J., Determination of cohesive parameters for a mixed-mode cohesive zone model, Int J Adhes Adhes, 30 (2010) 322-8.

[28] Chaves F.J.P., da Silva L.F.M., de Moura M.F.S.F., Dillard D.A., Esteves V.H.C., Fracture Mechanics Tests in Adhesively Bonded Joints: A Literature Review, The Journal of Adhesion, 90 (2014) 955-92.

[29] Oberg E., McCauley C.J., Machinery's handbook : a reference book for the mechanical engineer, designer, manufacturing engineer, draftsman, toolmaker, and machinist, 29th ed. ed., Industrial Press, New York, 2012.

[30] Huntsman, Araldite 2020 (XW 396 / XW 397) - Technical Data Sheet, Basel, 2007, http://www.farnell.com/datasheets/1640467.pdf?_ga=2.73488404.723075601.1565261557-238420828.1565261557, Accessed: 08/08/2019

[31] Huntsman, Araldite 2047-1 -Technical Data Sheet, Basel, 2010, https://www.intertronics.co.uk/wp-content/uploads/2016/01/Araldite-2047-1.pdf, Accessed: 08/08/2019

[32] Katsivalis I., Thomsen O.T., Feih S., Achintha M., Strength evaluation and failure prediction of bolted and adhesive glass/steel joints, Glass Structures & Engineering, 3 (2018) 183-96.

[33] da Silva L.F.M., Campilho R.D.S.G., Advances in Numerical Modelling of Adhesive Joints, Springer-Verlag Berlin Heidelberg, Berlin, 2012.

[34] Campilho R.D.S.G., Banea M.D., Neto J.A.B.P., da Silva L.F.M., Modelling adhesive joints with cohesive zone models: effect of the cohesive law shape of the adhesive layer, Int J Adhes Adhes, 44 (2013) 48-56.

[35] Sorensen B.F., Jacobsen T.K., Determination of cohesive laws by the J integral approach, Engineering Fracture Mechanics, 70 (2003) 1841-58.

[36] Sorensen B.F., Kirkegaard P., Determination of mixed mode cohesive laws, Engineering Fracture Mechanics, 73 (2006) 2642-61.

[37] Högberg J.L., Stigh U., Specimen proposals for mixed mode testing of adhesive layer, Engineering Fracture Mechanics, 73 (2006) 2541-56.

[38] De Moura M.F.S.F., Gonçalves J.P.M., Chousal J.A.G., Campilho R.D.S.G., Cohesive and continuum mixed-mode damage models applied to the simulation of the mechanical behaviour of bonded joints, Int J Adhes Adhes, 28 (2008) 419-26.

[39] Campilho R.D.S.G., Banea M.D., Neto J.A.B.P., da Silva L.F.M., Modelling of Single-Lap Joints Using Cohesive Zone Models: Effect of the Cohesive Parameters on the Output of the Simulations, The Journal of Adhesion, 88 (2012) 513-33.

[40] Domingues N.R.E., Campilho R.D.S.G., Carbas R.J.C., da Silva L.F.M., Experimental and numerical failure analysis of aluminium/composite single-L joints, Int J Adhes Adhes, 64 (2016) 86-96.

[41] Campilho R.D.S.G., de Moura M.F.S.F., Ramantani D.A., Morais J.J.L., Domingues J.J.M.S., Buckling Behaviour of Carbon–Epoxy Adhesively-Bonded Scarf Repairs, Journal of Adhesion Science and Technology, 23 (2009) 1493-513.

[42] Katsivalis I., Feih S., Thomsen O.T., Achintha M., Failure Prediction and Optimal Selection for Glass/Steel Adhesive Joints, Manuscript submiited for publication, Currently in revision, (2019).